Journal of Nuclear Medicine, published on October 27, 2016 as doi:10.2967/jnumed.116.180992

SYMPATHETIC INNERVATION OF COLD-ACTIVATED BROWN AND WHITE FAT IN LEAN YOUNG ADULTS

Otto Muzik [1,2], Tom J. Mangner[1], William R. Leonard[3],

Ajay Kumar[1], James G. Granneman[4,5]

Departments of Pediatrics[1], Radiology[2], Wayne State University School of Medicine, Detroit, MI, USA

Department of Anthropology[3], Northwestern University, Evanston, IL, USA

Center for Molecular Medicine and Genetics,[4] Center for Integrative Metabolic and Endocrine Research[5] and Family Medicine, Wayne State University School of Medicine, Detroit, MI, USA

Corresponding author:

Otto Muzik, PhD
PET Center
Children's Hospital of Michigan
3901 Beaubien Blvd
Detroit, MI, 48201 - USA
Tel: 313-993-2616
e-mail: otto@pet.wayne.edu

Running Title: Sympathetic innervation of BAT and WAT

Abstract word count: 347
Main text word count: 5032
Figures: 6
Tables: 2

Key-words: Brown fat, subcutaneous fat, sympathetic innervation, HED PET imaging

ABSTRACT

Objective: Recent work in rodents has demonstrated that basal activity of local sympathetic nervous system is critical for maintaining brown adipocyte phenotypes in classic brown (BAT) and white adipose tissue (WAT). Accordingly, we sought to assess the relationship between sympathetic innervation and cold-induced activation of BAT and WAT in lean young adults. **Methods:** Twenty adult lean normal subjects (10F/10M, 23.3 ± 3.8 years, BMI = 23.7 ± 2.5) underwent 11C-meta-hydroxyephedrin (HED) and 15O-water PET imaging at rest and following exposure to mild cold (16^{o}C) temperature. In addition, 18F-fluorodeoxyglucose (FDG) images were obtained during the cold stress condition to assess cold-activated BAT mass. Subjects were divided into two groups (High-BAT, Low-BAT) based on the presence of FDG tracer uptake. Blood flow and HED retention index (RI, an indirect measure of sympathetic innervation) were calculated from dynamic PET scans at the location of BAT and WAT. Whole body daily energy expenditure (DEE) during rest and cold stress was measured by indirect calorimetry. Tissue level oxygen consumption (MRO2) was determined and used to calculate the contribution of cold-activated BAT and WAT to daily DEE. **Results:** FDG uptake identified subjects with high and low levels of cold-activated BAT mass (High-BAT, 96 ± 37g; Low-BAT 16 ± 4g). HED RI under thermoneutral conditions significantly predicted FDG uptake during cold stress (R^2 = 0.68, $p<0.01$). In contrast to the significant increase of HED RI during cold in BAT (2.42±0.85 vs. 3.43±0.93, p=0.02), cold exposure decreased the HED RI in WAT (0.44±0.22 vs. 0.41±0.18) as a consequence of decreased perfusion (1.22±0.20 vs. 1.12±0.16 ml/100g/min). The contribution of WAT to whole body DEE was ~150 kcal/day at rest (149±52 kcal/day) which decreased to ~100 kcal/day during cold (102±47 kcal/day). **Conclusion:** The level of sympathetic innervation, as determined by HED RI, can predict levels of functional BAT. Overall, blood flow is the best independent predictor of HED RI and FDG uptake across thermoneutral and cold conditions. In contrast to BAT, cold stress reduces blood flow and FDG uptake in subcutaneous WAT, indicating that the physiological response is to reduce heat loss rather than to generate heat.

INTRODUCTION

The main function of brown adipocytes in mammals is the generation of heat in response to cold stress. In addition to comprising the parenchyma of classic interscapular brown adipose tissue (BAT), brown adipocytes (BA) can be found dispersed in various white adipose tissue depots (*1,2*). Cold stress is a powerful physiological stimulus for activating parenchymal BA cells in BAT as well as recruiting their appearance in typical white adipose tissue (WAT) depots (*3,4*). Recent work has clearly established the presence of BA cells in the supraclavicular region of humans (*5,6*). Whether these cells more closely resemble typical BA cells found in classic BAT or BA cells that appear in WAT is controversial (*2,7*). Nonetheless, the functional activation of BA cells can be clearly induced by mild cold stress in humans, although the presence and abundance of BAT varies greatly for reasons that are presently unclear.

The sympathetic nervous system is the major regulator of cold-induced BAT activity and mass in rodents (*8,9*). Perhaps not surprisingly, the recruitment of BA cells in WAT depots by cold stress or direct beta3 adrenergic activation is correlated with the density of sympathetic innervation of individual fat pads (being greatest in subcutaneous and least in visceral fat) (*1,8*). Importantly, chronic sympathetic denervation of WAT pads impairs the ability of direct beta3 receptor agonists to induce the BA phenotypes in WAT, indicating that the ability of phenotypic flexibility of subcutaneous WAT depends on ongoing sympathetic activity (*10*). On the basis of these data, we hypothesized that variations in the presence of supraclavicular BAT in humans will be directly related to the level of sympathetic innervation.

The norepinephrine analog 11C-meta-hydroxyephedrine (HED) has been widely used in PET imaging to map the regional sympathetic innervation of the heart (*11,12*) and other tissues (*13*). As a structural analog of the neurotransmitter norepinephrine, HED is taken up by the norepinephrine transporter (NET) and accumulates in sympathetic neurons. Thus, the kinetics of HED can be used to assess

tissue NET activity and by inference, the density of sympathetic innervation. Accordingly, the objectives of this paper were to determine the utility of HED in assessing sympathetic innervation in human BAT and to test whether HED uptake at rest could predict the level of metabolic activation of BAT during cold stress. In addition, we assessed the contribution of subcutaneous and visceral WAT to cold-induced energy expenditure in lean young adults.

MATERIALS AND METHODS

Subjects

A total of 20 adult lean normal subjects (10F/10M, 23.3 $\pm$ 3.8 years, BMI = 23.7 $\pm$ 2.5) were studied. The study was approved by the Wayne State University Institutional Review Board and written consent was obtained from all participants. All subjects underwent ^{11}C-meta-hydroxyephedrin (HED) and 15O-water PET imaging at rest and following exposure to mild cold (16^{o}C). In addition, 18F-fluorodeoxyglucose (FDG) images were obtained during the cold stress condition to assess the presence of activated BAT. Mild cold exposure was applied using a specialized whole-body garment, which incorporates a network of small-diameter plastic tubing (Allen Vangard, Inc., Ottawa, CA) (**Supplemental Fig. 1**). Details with respect to the cooling procedure are provided in the Supplemental Data file. Subjects were closely monitored during the cold exposure period for signs of shivering. In addition to monitoring the skin temperature, subjects reported every 5 minutes about his/her subjective feeling of cold and if shivering was likely to occur, the water temperature in the garment was raised. Post-experimental debriefing verified that all subjects experienced the cold condition as a pain-free cold sensation without substantial discomfort.

HED kinetic model

Previous mechanistic studies of the HED tracer have established high neuronal selectivity, long neuronal retention times and a correlation between tissue retention of tracer and tissue norepinephrine concentration (*14*). On the basis of previous studies in animals (*13*) and humans (*15*), a comprehensive compartmental model of myocardial HED kinetics has been developed (**Supplemental Fig. 2**). Because the NET transport rate of HED (k3) is much faster than the rate of clearance back into plasma ($k3 \gg k2$), most of the HED molecules delivered from plasma to the extracellular space are rapidly transported into the neurons. This causes the neuronal uptake of HED to be rate limited by delivery from plasma into interstitium (K1), rather than by NET transport (k3). Supporting this view, HED retention has been previously shown to be flow-dependent in the dog heart (*16*). Moreover, due to high lipophilicity (log P = 0.31), the HED tracer continuously leaks from sympathetic nerve terminals during the PET study (k4) (*16*). Thus, HED tissue retention is a complex function of tracer delivery and washout, both strongly affected by blood flow. In fact, the situation is even more complicated since the relationship between HED retention and blood flow changes for different level of norepinephrine release in the synaptic cleft due to competitive inhibition of HED uptake at the NET. Unfortunately, correcting for flow effects is not straightforward even if one has flow estimates available. To do so would require a detailed knowledge of the dependence of the tracer's retention on flow in order to perform a proper "flow normalization" of the HED retention values, information that is unavailable.

PET Data Acquisition

All subjects were scanned using a GE Discovery STE PET/CT scanner in 3D mode, except for the 15O-water scans, which were performed in 2D mode in order to decrease contribution of scatter from outside of the field-of-view (FOV). Initially, a venous catheter was established for tracer injection. One venous blood sample (0.5cc total) was collected to determine hematocrit levels; moreover arterial oxygen saturation (pSat) was monitored during the whole protocol using a Dinamap ProCare 400 monitor (GE, Milwaukee, WI). The protocol started with two low-level CT scans

(100kVp, 60mA) for attenuation correction; one at the location of the neck/shoulder region (also including the ascending aorta inferior to the aortic arch) and the other at the level of subcutaneous WAT in the lower abdomen (including the descending aorta). Following acquisition of the transmission scans, 15O-water (1.1 GBq) was injected as a slow bolus over 20s and a 2min dynamic PET scan of the neck/shoulder region was obtained (60 x 2s). Following a 10 min period to allow for decay of tracer (15O half-life is 2min), the 15O-water scan was repeated with the lower abdomen in the FOV. Subsequently the patient was repositioned with the neck/shoulder region in the FOV and following a 10 min period to allow for tracer decay, HED (370 MBq) was injected as a slow bolus over 20s. Coinciding with the tracer injection, a dynamic scan was initiated (12 x 10s, 3 x 60s, 4 x 300s). At the conclusion of the dynamic scan the patient was repositioned with the lower abdomen in the FOV and a static scan (8min) of abdominal WAT was obtained. During the entire baseline protocol, subjects were kept in a thermoneutral condition by maintaining the suit water temperature at 31-34^{o}C. Following the baseline protocol, subjects were exposed to mild cold temperature for the rest of the study by changing the circulating water temperature to 15-17^{o}C. After a cooling period of at least one hour duration, the baseline protocol was repeated. At its conclusion, the FDG tracer (150 MBq) was injected and following a 50min uptake period, a four bed-position PET/CT scan was acquired, covering the torso from the shoulder to the lower abdomen. All PET emission data was corrected for attenuation, scatter, and random events, and then iteratively reconstructed into 128x128x47 matrices (voxel dimensions, 5.47 x 5.47 x 3.27 mm) using the ordered subset expectation maximization (OSEM) algorithm provided by the manufacturer (2 iterations, 20 subsets, and post-processing Gaussian filter with 6.0 mm FWHM). The final spatial resolution of the image volumes was ~7mm FWHM.

Image Data Processing and Analysis

In order to calculate blood flow and tracer retention, the arterial input functions needs to be known. The validity of an image-derived input function obtained from the ascending aorta (AA) for accurate quantification of myocardial

perfusion has been shown in several 15O-water studies that compared flow values obtained using the image-derived input function with those determined using arterial blood sampling (*17,18*). Using the AMIDE software, a 3D region-of-interest (ROI, 1cm diameter) was defined over the AA and spillover from the left atrium was avoided by considering only planes in which the left atrium was not visible. The resulting time-activity curve was subsequently corrected for partial volume effects by taking into account the diameter of the AA obtained from CT (2.3 $\pm$ 0.3cm) and the full-width-at half maximum of the reconstructed PET images (*19*). In order to extrapolate the AA time-activity curve beyond the initial 25min, the curve was fitted with a tri-exponential function and the slowest exponential was used for continuation of the input function up to 40min p.i. An analogous approach was used for the abdominal scans using the descending aorta (DA). It was shown that this method is in good agreement with the arterial function, as the DA is relatively free of spillover from other organs and extends from the upper thorax to the lower abdomen (*20*). The ROIs representing supraclavicular BAT as well as subcutaneous and visceral WAT were defined in CT images based on the density of adipose tissue (−250 to −50 Hounsfield units, HU). ROIs representing subcutaneous WAT (WAT) were defined at the level of the lower abdomen superior to the hip joint, whereas visceral WAT (viscWAT) ROIs were defined below the kidneys. A ROI at the location of the deltoid muscle was assumed to be representative for muscle tissue. BAT was considered as activated if there were areas of tissue that were more than 5 mm in diameter and had a minimal standard uptake value (SUV, defined as tracer concentration in MBq/cc normalized to injected activity (MBq) per weight (g)) of FDG of at least 2.0. BAT volume was determined by thresholding both the CT image volume (-250 < HU < -50) and the FDG volume (SUV > 2.0) and then applying the logical AND operation to the 2 masks, followed by removal of all areas that were smaller than 0.125 cm^3. The volume of BAT ROIs (cm^3) was converted into weight (g) by assuming a density of 0.90 g/cm^3. Regional time-activity curves were derived from 15O-water and HED scans and blood flow F(ml/g/min) and HED retention index (RI) was estimated from the following equations

$$PET(t_i) = F\int_0^{t_i} C_{AA}(u)\cdot e^{-\frac{F}{\lambda}(t_i-u)}du \qquad RI = C^{HED}_{(30-40)} \Big/ \int_0^{40} C_{AA}(u)du \tag{1}$$

where PET(ti) is the measured time-activity curve (uCi/cc) obtained from the dynamic 15O-water injection and λ is the partition coefficient of tissue to blood (0.92 ml/g). Finally, the retention index (RI) in tissue was calculated as the quotient between the average HED tracer concentration in BAT/WAT tissues 30-40min p.i. and the integral of HED tracer concentration in blood (*21*). As mentioned earlier, because of the dynamic recycling of the HED tracer at the neuronal membrane, the HED RI is a complex function of both blood flow and norepinephrine concentration. Although an exact "flow normalization" of the HED RI is problematic, we applied an approximate blood flow correction of BAT HED uptake by dividing the RI(%) by the independently measured perfusion values (ml/100g/min). This flow-corrected RI in BAT is denoted as RI_{fc} and is presented in addition to the non-corrected RI. Because blood flow in subcutaneous WAT is similar at cold and during thermoneutral condition (*22,23*), HED retention in WAT can be regarded as a reflection of the number or integrity of norepinephrine terminals (*15*) in WAT during these states. Finally, using the previously established OEF for BAT (0.50), WAT (0.40) and muscle (0.30) (*23*), the metabolic rate of oxygen (MRO_2; ml/100g/min) in tissue was calculated as the product of blood flow (F; ml/100g/min), OEF (unitless) and the arterial oxygen concentration (cO_2; mlO_2/100ml) as follows

$$MRO_2(\frac{ml}{g\,\min}) = F(\frac{ml}{g\,\min})\cdot OEF\cdot cO_2(\frac{mlO_2}{100ml}) \tag{2}$$

$$cO_2(\frac{mlO_2}{100ml}) = (\frac{HCT}{3})\cdot(1.36\,pSat) + (0.0031\,pO_2(torr)) \tag{3}$$

where cO_2 is derived from the patient's arterial oxygen saturation (pSat; %), the hematocrit (HCT) and the partial pressure of O_2 (pO_2), which is calculated from the measured pSat according to Severinghaus' formula and the exact inversion by Ellis

(*24*). Finally, the Daily Energy Expenditure (DEE; kcal/day) was calculated from the obtained MRO_2 and the weight of BAT according to the formula

$$DEE(\frac{kcal}{day}) = MRO_2(\frac{ml}{g\,\min}) \cdot weight(g) \cdot 0.0048(\frac{kcal}{ml}) \cdot 1440(\frac{\min}{day}) \quad (4)$$

where the conversion factor between kcal and ml O_2 was assumed for an RQ of 0.80 (*25*). Finally, we assume 1g ~ 1ml.

Whole body Indirect Calorimetry

Measurement of energy expenditure (kcal/day) under resting and cold conditions was performed using the MedGraphics VO2000 Portable Metabolic Testing System (St. Paul, MN). For both conditions, subjects were measured while lying in a relaxed position, in a fasted state for at least 6 hours. Subjects were fitted with neoprene face masks, and all measurements were taken using the low flow pneumotachs. Heart rate (beats/min), oxygen consumption (VO_2, l/min), carbon dioxide production (VCO_2, l/min) and respiratory quotient (VCO_2/VO_2) were all measured for 10 minutes. Whole body DEE was then calculated based on the Weir equation (*26*) using the BreezeSuite software (Version 6.0; MedGraphics).

Statistical Analysis

Data are reported as mean $\pm$ SD and all analysis was performed with the use of SPSS software version 21 (IBM Corp., Armonk, NY). FDG uptake in BAT following cold exposure was highly variable, with a few subjects (all females) showing extensive uptake in the cervical–supraclavicular depots. A histogram of cold-activated BAT mass showed two distinct peaks with maxima at 10-20g and at 80-90g (Supplemental Fig. 3). To account for the bimodal distribution, subjects were divided into two groups (High-BAT and Low-BAT), with the threshold separating the two groups set to 20 g of activated BAT. Normally distributed continuous variables were compared between the two groups using an independent sample t-test and non-normally distributed continuous variables using the Mann-Whitney U-test. Finally, correlations

between variables were assessed using Pearson's r. All reported p-values are two-tailed and values less than 0.05 were considered to indicate statistical significance.

RESULTS

Descriptive Statistics

Table 1 shows descriptive statistics characterizing the subject population. The study population consisted of lean (BMI = 23.0 $\pm$ 2.6 kg/m^2) young (25.1 $\pm$ 5.2 years of age) controls (10M/10F) without any indication for cardiovascular or diabetic disease. We observed a wide variation in cold-activated BAT ranging from 0 to 182g, characterized by a bimodal distribution. Following cold exposure, about 2/3 of the subjects showed relatively high BAT activation (~100g, High-BAT group), whereas 1/3 of the subjects displayed low BAT activation (< 20g, Low-BAT group). The SUVmax determined in the High-BAT group was significantly higher than that measured in the Low-BAT group (19.5$\pm$8.0 vs. 7.2$\pm$1.7; $p < 0.01$). Moreover, the prevalence of significant amount of activated BAT was higher in females (8/10) as compared to males (5/10) – the average activated BAT mass was determined as 88 $\pm$ 55g in females whereas it was 50 $\pm$ 38g in males ($p = 0.12$). Conforming to the measured BMI values, the visceral fat area was found to be higher in the Low-BAT group, despite the virtually identical body fat percentage.

As expected from previous work (*4,5,27*), the two groups showed different responses in their DEE to mild cold exposure. In the High-BAT group the baseline DEE was lower than in the Low-BAT group, however during mild cold exposure the DEE increased by about 17% (from 1349$\pm$309 to 1689$\pm$463 kcal/day, $p = 0.015$). In contrast, cold exposure failed to increase energy expenditure in the Low-BAT group (change 1712$\pm$337 to 1722$\pm$312 kcal/day, **Table 1**). Moreover, whereas absolute changes in DEE were always positive in the High-BAT group (range 48 – 783, mean =

340 ± 380 kcal/day), DEE changes in the Low-BAT group varied considerably (range -496 to 538, mean = 9 ± 361 kcal/day).

Finally, the respiratory quotient (VCO_2/VO_2) was marginally lower in the High-BAT as compared to the Low-BAT group (0.85 ± 0.06 vs. 0.91 + 0.11; p = 0.16), suggesting greater levels of resting fat oxidation in this group (*28*). However, RQ values were not significantly affected by cold stress.

HED uptake in supraclavicular BAT

We determined a significant increase in HED RI in supraclavicular BAT of High-BAT subjects in both the absence and presence of cold stress. Moreover, HED RI corresponded to cold-activated FDG tracer uptake (**Fig. 1**). More specifically, we observed a highly significant correlation between the RI_{rest} and the amount of BAT mass (R^2 = 0.68, p < 0.01), indicating that HED uptake during thermoneutral condition is a good predictor of cold-activated BAT mass. RI_{cold} was also highly correlated with FGD uptake (R^2 = 0.73, p < 0.01) (**Fig. 2A**). Moreover, as predicted based on the characteristics of the HED tracer, we found that blood flow and RI_{rest} (R^2 = 0.48, p =0.04) as well as RI_{cold} (R^2 = 0.72, p < 0.01, **Fig. 2B**) were highly correlated. In addition, a significant correlation was found between the RI_{rest} and RI_{cold} (R^2 = 0.62, p < 0.01). Taken together, our results indicate that the abundance of NETs, and by inference the level of sympathetic innervation, in BAT predicts the magnitude of cold-induced activation in this tissue.

HED uptake in subcutaneous WAT

In contrast to the significant increase of HED RI in supraclavicular BAT following cold exposure, HED RI in both subcutaneous and visceral WAT as well as muscle was similar during cold and neutral conditions (**Fig. 3A**). Interestingly, HED RI in visceral WAT was found to be about twice that in subcutaneous WAT (**Table 2**). In addition, whereas the increase in HED RI at the location of supraclavicular BAT following cold exposure was increased during cold (**Fig. 3B**), we determined a

consistent decrease (albeit small) in HED RI following cold exposure at the location of subcutaneous WAT (**Fig. 3C**). These data suggest that even in subjects with significant amount of cold-activated supraclavicular BAT, the contribution of WAT to overall energy expenditure is modest at best. The decrease in HED RI observed in both subcutaneous WAT and visceral WAT is most likely a consequence of lower blood flow in these tissues during cold exposure.

Relationship between blood flow and sympathetic innervation

In order to assess the relationship among blood flow, sympathetic innervation and glucose uptake in supraclavicular BAT and subcutaneous WAT, O15-water derived flow values, HED-derived RI as well as FDG SUV measures were compared. The **Fig. 4** illustrates this relationship, indicating a tight association among these three physiological parameters. Moreover, we determined a highly significant correlation between cold-activated BAT-mass and the flow-corrected RI (RI_{fc}) under thermoneutral conditions ($R^2 = 0.54$, $p < 0.01$, **Fig. 5**), but not during cold stress ($R^2 = 0.13$, $p > 0.05$). More importantly, analysis of blood flow and uncorrected HED RI at rest by multiple regression indicate that both blood flow and HED RI_{rest} were significant independent predictors of BAT mass (partial regression of 0.50 for blood flow and 0.17 for HED ($p = 0.012$).

Energy expenditure in BAT and WAT

Based on our previous work that established values for the oxygen extraction fraction (OEF) at thermoneutral and cold conditions (*22*) and the measured blood flow values, we calculated DEE in supraclavicular BAT and subcutaneous WAT (**Fig. 6**). An OEF value of 0.50 was used for supraclavicular BAT, whereas an OEF value of 0.40 was used for subcutaneous WAT (*22*). Our current results confirm our previous findings indicating a very low contribution of supraclavicular BAT to DEE of less than 20 kcal/day, even for subjects with relatively large amount of activated BAT (96±37g in the High-BAT group). Our findings indicate a DEE of ~7kcal/day (range 1.6 – 12 kcal/day) at thermoneutral condition, which increases to between 10-20 kcal/day

(range 4.7 – 29 kcal/day) following cold exposure (**Fig. 6A**). Specifically, in the High-BAT group we determined a significantly increased DEE in BAT following cold exposure (7.5±5.3 vs. 10.9±7.6 kcal/day, $p < 0.01$), whereas in the Low-BAT group the DEE at the location of BAT was much lower and similar during thermoneutral and cold conditions (0.70±0.66 vs. 0.91±0.64 kcal/day). Although the blood flow and metabolic rate was found to be much lower in subcutaneous WAT, due to the large mass (17.4±4.9kg, see **Table 1**) the associated DEE was found to be considerable (~150kcal/day). Interestingly, although DEE in WAT was found to be similar at thermoneutral condition in the High-BAT and Low-BAT groups (150±72 vs. 148±39 kcal/day), it was substantially decreased in both groups during cold exposure, most likely due to decreased perfusion. In the High-BAT group the decrease was ~25% (to 115±55 kcal/day) while in the Low-BAT group the decrease was ~40% (to 89±40 kcal/day, $p < 0.01$, **Fig. 6B**).

DISCUSSION

The aim of this study was to quantify sympathetic innervation in both supraclavicular BAT and subcutaneous WAT in lean young adults during both thermoneutral and cold exposure conditions as well as to relate sympathetic innervation in these tissues to blood flow and glucose uptake. The data presented here indicate that the presence of cold-activated BAT can be predicted by HED tracer uptake during thermoneutral conditions.

There are several key outcomes from this work: Firstly, we determined a linear relationship between blood flow (ml/100g/min) and sympathetic innervation (RI%) in both BAT and WAT as measured by HED PET imaging, reflecting the well-established coupling of blood flow with sympathetic innervation (*29*). Secondly, whereas sympathetic innervation (and associated blood flow) increases following cold exposure in supraclavicular BAT, both these measures slightly decreased in subcutaneous WAT, resulting in a decreased contribution of WAT to whole body DEE

during the cold state. The observed cold-induced vasoconstriction in WAT suggests decreased heat production, as it is unlikely that an increase in thermogenic capacity of subcutaneous WAT would not be accompanied by a simultaneous increase in perfusion in order to supply fuel and oxygen as well as to dissipate the generated heat throughout the body. Thus, our findings point to a situation in which WAT appears to play an insulative role rather than a metabolic one in combatting cold stress, with a physiological response that targets reduction of heat loss rather than generation of heat. Interestingly, the decrease in WAT DEE during cold exposure was found to be somewhat lower in the High-BAT group as compared to the Low-BAT group, however the relevance of this finding is presently unclear.

WAT oxidative metabolism

Our findings indicate that the resting oxygen metabolic rate (MRO_2) of subcutaneous WAT is 0.13 $\pm$ 0.04 ml/100g/min at rest and decreases to 0.09 + 0.03 ml/100g/min during mild cold. These values result in a specific metabolic rate in subcutaneous WAT of ~7.5 kcal/kg/day, which is close to the previously estimated metabolic rate of ~5 kcal/kg/day based on a mechanistic model (*30,31*). Moreover, our MRO_2 values for subcutaneous WAT compare well with those in muscle which have been reported as ~0.2 ml/100g/min (equivalent to ~12 kcal/kg/day), reflecting the expected rank order of MRO_2 in tissues. In contrast, the observed MRO_2 values for visceral WAT in the range of 0.25 – 0.30 ml/100g/min (equivalent to 15 – 18 kcal/kg/day) appears to be high, especially in comparison with muscle MRO_2. Although an increased metabolic rate in visceral WAT cannot be completely excluded, the measurement of PET activity at the location of visceral WAT is problematic due to the small sampled volumes that are subject to spillover from adjacent organs. It has to be noted that this situation is in stark contrast to the sampling of subcutaneous WAT depots, which are much larger and therefore allow definition of time-activity curves that are free of partial volume effects.

WAT and whole body energy expenditure

It is now well established that cold stress increases the oxidative metabolism in human BAT depots (*32*). We and others (*33*) have observed that cold-induced increases in whole body energy expenditure (average of ~220 kcal/d in the present study) is strongly correlated with the presence of cold-activated BAT depots. Furthermore, activation of human BAT depots appears to be selectively induced by cold stress, but not by nonselective sympathomimetic activation (*4*). Nonetheless, these PET-defined BAT depots account for less than 5% of the total cold-induced increase in metabolism, an observation supported by other recent reports (*34*,*35*). Moreover, these investigators have also presented data that suggests that deep, centrally located muscles of the neck, back and inner thigh are the greatest contributors to cold-induced thermogenesis via activation of muscle shivering on a microscale level, with BAT possibly assuming a more endocrine role.

Due to decreased blood flow in subcutaneous WAT during cold exposure, it is unlikely that WAT directly contributes to cold-induced whole body energy expenditure. Nevertheless, our data suggests a higher thermogenic capacity of WAT in subjects with large amount of activated BAT (High-BAT group) as compared to subjects with low amount of BAT (Low-BAT group), suggesting a common physiological network mediating the effect of NST in both tissues. The decrease in the contribution of WAT to DEE was found to be about twice as large in the Low-BAT group as compared to the High-BAT group (~60 vs. ~30 kcal/day), leaving open the interpretation that this difference in WAT DEE involves activation of "beige" adipocytes that can be recruited by cold stress or adrenergic agonists, but that are too diffuse to be imaged by PET.

Relationship between blood flow and FDG uptake

The accumulation of FDG in tissues is generally believed to represent the rate of glycolytic metabolism. Delivery of the tracer to the tissue is obviously essential and blood flow may play an important role in the ultimate FDG tissue uptake observed. The relationship between blood flow and FDG tissue uptake has been extensively

studied in human tumors using PET imaging (*36,37*). These studies have clearly demonstrated a strong relationship between blood flow and SUV or metabolic rate of glucose with correlation coefficients in the range of 0.7-0.8 (*36,38*). It is interesting to note that the blood flow range in these studies was almost identical to that observed in our BAT studies (5 – 30 ml/100g/min). Conceptually, the strong relationship between blood flow and FDG tissue uptake is a consequence of the fact that the unidirectional inflow parameter for FDG (K1) is highly correlated with blood flow (r=0.84), whereas the fraction of FDG in cytosol being metabolized (k3/(k2+k3)) is not related to blood flow (r<0.1) (*36*). Thus, given the fact that the K-complex is the product of K1 and the fraction of metabolizeable glucose inside the cell (= k3/(k2+k3)), the obtained glucose metabolic rate (and SUV) are directly related to blood flow. Further support for the strong correlation between FDG tissue uptake and blood flow stems from studies that compare cerebral perfusion based on arterial spin labeling MRI (ASL-MRI) with FDG PET uptake (*39,40*). These authors concluded that FDG-PET and ASL-MRI identify similar regional abnormalities and have comparable diagnostic accuracy. Thus the observed high SUVs in BAT might reflect primarily increased blood flow with a relatively low increase in metabolic activity, reflected by the accompanying low oxygen consumption of BAT tissue (*22*).

Along the same lines, given the observed significant increase in BAT perfusion during cold (~7ml/100g/min equal to ~10L/100g/d) and the fact that the temperature of blood is equal to the core body temperature (37^{o}C or 98.6^{o}F), a significant amount of additional heat is transported from the core to BAT during cold exposure. The amount of additional heat energy (kcal) reaching BAT during cold exposure can be calculated using the heat capacity of blood (3.49 kJ/kg/^{o}C) and assuming a conservative core/surface temperature gradient of ~3^{o}C (*41*), yielding a value of ~25 kcal/day for a BAT mass of 100g. Thus, the heat supplied to BAT by blood flow from the core likely exceeds the heat generated in BAT by a factor of 3. These observations suggest that an important function of BAT innervation might be the redistribution of core heat to critical regions in the supraclavicular and spinal

regions. In this regard, norepinephrine infusion was recently shown to dramatically increase blood flow to murine BAT in the absence of UCP1-mediated thermogenesis (*42*).

Comparison with other work

Because tissue MRO_2 (and the associated energy expenditure) is the product of blood flow and oxygen extraction, blood flow sets the upper limit of tissue oxygen consumption. In this regard, we note that the here reported cold-induced increase in supraclavicular BAT blood flow is nearly identical to that reported by other investigators (e.g. *27*). Thus, based on available blood flow data one can deduce that acutely-activated human BAT contributes very little to cold-induced energy expenditure, even if one assumes 100% OEF. These values are consistent with recent tracer experiments showing that the energy content of glucose (*27*) or nonesterified fatty acids (*32*) taken up by active BAT is trivial when compared to cold-induced energy expenditure (*33*). Finally, the energy content of cold-induced glucose uptake in human BAT was reported by various investigators (*6,27,34*) to amount to less than 10 kcal/d if fully oxidized, in agreement with our findings.

The existence of cold-induced thermogenesis that is independent of BAT is well documented, particularly in warm-adapted animals (*43,44*). These sites of thermogenesis remain poorly defined, but could involve elevated metabolism in muscle (*45*). The defense against cold is likely an innate property of mammals, and "browning" of subcutaneous WAT was originally one more layer of defense against the cold, in addition to other mechanisms that mediate NST, such as futile cycling of the Ca^{2+}-ATPase (SERCA) pump in muscle (*46*). Our data suggests that during human evolution the importance of WAT browning for protection against acute cold diminished, but still might play a role in seasonal adaptation to cold. Despite the paucity of studies investigating seasonal changes in whole body energy expenditure, there are reports of higher metabolic rates during the winter as compared to summer (*47-49*). Thus, even though seasonal changes of WAT thermogenesis were not the

focus of our study, such changes are of particular interest, since they indicate a physiologic response to colder weather even in a modern society, where indoor temperature is regulated and without the provocative stimulated cooling that is usually required to stimulate BAT.

Conclusion

In summary, the main result of our study is that the contribution of subcutaneous WAT to whole body energy expenditure during acute cold exposure is negative. The cold-induced decrease in WAT energy expenditure is less pronounced in subjects with high amount of activated supraclavicular BAT, leaving open the possibility that in these subjects "beige" adipocytes exist that can be activated by long-term (seasonal) exposure to cold. Finally, our data indicates that differences in the level of sympathetic innervation are, at least partially, responsible for the widely observed variability of cold-activated BAT mass in lean subjects.

DISCLOSURE

This study was supported by a grant from NIDDK (R01DK102455-01).

REFERENCES

1. Cinti S. Between brown and white: novel aspects of adipocyte differentiation. *Ann Med.* 2011;43:104-115.

2. Sharp LZ, Shinoda K, Ohno H et al. Human BAT possesses molecular signatures that resemble beige/brite cells. *PLoS One*. 2012;7:e49452.

3. Dempersmier J, Sambeat A, Gulyaeva O et al. Cold-inducible Zfp516 activates UCP1 transcription to promote browning of white fat and development of brown fat. *Mol Cell*. 2015;57: 235-246.

4. Cypess AM, Chen YC, Sze C et al. Cold but not sympathomimetics activates human brown adipose tissue in vivo. *Proc Natl Acad Sci USA*. 2012;109:10001-10005.

5. Cypess AM, Lehman S, Williams G et al. Identification and importance of brown adipose tissue in adult humans. *N Engl J Med*. 2009;360:1509-1517.

6. Virtanen KA, Lidell ME, Orava J, et al. Functional brown adipose tissue in healthy adults. *N Engl J Med*. 2009;360:1518–1525.

7. Sidossis L, Kajimura S. Brown and beige fat in humans: thermogenic adipocytes that control energy and glucose homeostasis. *J Clin Invest*. 2015;125:478–486.

8. Murano I, Barbatelli G, Giordano A, Cinti S. Noradrenergic parenchymal nerve fiber branching after cold acclimatisation correlates with brown adipocyte density in mouse adipose organ. *J Anat*. 2009;214:171-178.

9. Morrison SF, Ramamurthy S, Young JB. Reduced rearing temperature augments responses in sympathetic outflow to brown adipose tissue. *J Neurosci*. 2000;20:9264-9271.

10. Contreras GA, Lee YH, Mottillo EP, Granneman JG. Inducible brown adipocytes in subcutaneous inguinal white fat: the role of continuous sympathetic stimulation. *Am J Physiol Endocrinol Metab*. 2014;307:E793-799.

11. Raffel DM, Chen W, Sherman PS, Gildersleeve DL, Jung YW. Dependence of cardiac 11C-meta-hydroxyephedrine retention on norepinephrine transporter density. *J Nucl Med*. 2006;47:1490-1496.

12. Fricke E, Fricke H, Eckert S et al. Myocardial sympathetic innervation in patients with chronic coronary artery disease: is reduction in coronary flow reserve correlated with sympathetic denervation? *Eur J Nucl Med Mol Imaging*. 2007;34:206-211

13. Thackeray JT, Beanlands RS, Dasilva JN. Presence of specific 11C-meta-Hydroxyephedrine retention in heart, lung, pancreas, and brown adipose tissue. *J Nucl Med*. 2007;48:1733-1740.

14. Rosenspire KC, Haka MS, Van Dort ME et al. Synthesis and preliminary evaluation of carbon-11-meta-hydroxyephedrine: a false transmitter agent for heart neuronal imaging. *J Nucl Med*. 1990;31:1328-1334.

15. Raffel DM, Wieland DM. Assessment of cardiac sympathetic nerve integrity with positron emission tomography. *Nucl Med Biol*. 2001;28:541-559.

16. DeGrado TR, Hutchins GD, Toorongian SA, Wieland DM, Schwaiger M. Myocardial kinetics of carbon-11-meta-hydroxyephedrine: retention mechanisms and effects of norepinephrine. *J Nucl Med*. 1993;34:1287-1293.

17. Lubberink M, Harms HJ, Halbmeijer R, de Haan S, Knaapen P, Lammertsma AA. Low-dose quantitative myocardial blood flow imaging using 15O-water and PET without attenuation correction. *J Nucl Med*. 2010;51:575-580.

18. van der Veldt AA, Hendrikse NH, Harms HJ et al. Quantitative parametric perfusion images using 15O-labeled water and a clinical PET/CT scanner: test-retest variability in lung cancer. *J Nucl Med*. 2010;51:1684-1690.

19. Germano G, Chen BC, Huang SC, Gambhir SS, Hoffman EJ, Phelps ME. Use of the abdominal aorta for arterial input function determination in hepatic and renal PET studies. *J NucI Med*. 1992;33:613-620.

20. Ohtake T, Kosaka N, Watanabe T, et al. Noninvasive method to obtain input function for measuring tissue glucose utilization of thoracic and abdominal organs. *J Nucl Med*. 1991:32:1432–1438.

21. Allman KC, Wieland DM, Muzik O, Degrado TR, Wolfe ER Jr, Schwaiger M. Carbon-11 hydroxyephedrine with positron emission tomography for serial assessment of cardiac adrenergic neuronal function after acute myocardial infarction in humans. *J Am Coll Cardiol*. 1993;22:368-375.

22. Muzik O, Mangner TJ, Granneman JG. Assessment of oxidative metabolism in Brown Fat using PET imaging. *Front Endocrinol*. 2012;3:1-7.

23. Muzik O, Mangner TJ, Leonard WR, Kumar A, Janisse J, Granneman JG. 15O PET measurement of blood flow and oxygen consumption in cold-activated human brown fat. *J Nucl Med*. 2013;54:523-531.

24. Ellis RK. Determination of PO2 from saturation. *J Appl Physiol*. 1989;67(2):902-906.

25. Leonard WR. Measuring human energy expenditure and metabolic function: basic principles and methods. *J Anthropol Sci*. 2010;88:221-230.

26. Weir JB. New methods for calculating metabolic rate with special reference to protein metabolism. *J Physiol Lond*. 1949;109:1– 9.

27. Orava J, Nuutila P, Lidell ME et al. Different metabolic responses of human brown adipose tissue to activation by cold and insulin. *Cell Metab*. 2011;14:272-279.

28. McArdle WD, Katch FI, Katch VL. Exercise Physiology: Energy, Nutrition, and Human Performance (5th Edition) 2001. Philadelphia: Lippincott, Williams & Wilkins.

29. Guyenet PG. The sympathetic control of blood pressure. *Nat Rev Neurosci*. 2006; 7:335-346. Review.

30. Wang Z, Ying Z, Bosy-Westphal A et al. Evaluation of specific metabolic rates of major organs and tissues: comparison between men and women. *Am J Hum Biol*. 2011; 23: 333-338.

31. Elia, M. Organ and tissue contribution to metabolic rate. In: Kinney, JM.; Tucker, HN., editors. Energy Metabolism: Tissue Determinants and Cellular Corollaries. Raven Press 1992; New York: 61-80.

32. Ouellet V, Labbé SM, Blondin DP, et al. Brown adipose tissue oxidative metabolism contributes to energy expenditure during acute cold exposure in humans. *J Clin Invest*. 2012;122:545–552.

33. Yoneshiro T, Aita S, Matsushita M, et al. Brown adipose tissue, whole-body energy expenditure, and thermogenesis in healthy adult men. *Obesity*. 2011;19:13–16.

34. Din M, Raiko J, Saari T et al. Human brown adipose tissue [15O]O2 PET imaging in the presence and absence of cold stimulus. *Eur J Nucl Med Mol Imaging*. 2016 [Epub ahead of print]

35. Blondin DP, Labbé SM, Phoenix S et al. Contributions of white and brown adipose tissues and skeletal muscles to acute cold-induced metabolic responses in healthy men. *J Physiol*. 2015;593:701-714.

36. Zasadny KR, Tatsumi M, Wahl RL. FDG metabolism and uptake versus blood flow in women with untreated primary breast cancers. *Eur J Nucl Med*. 2003;30:274–280.

37. Mullani NA, Herbst RS, O'Neil RG, Gould KL, Barron BJ, Abbruzzese JL. Tumor blood flow measured by PET dynamic imaging of first-pass 18F-FDG uptake: a comparison with 15O-labeled water-measured blood flow. *J Nucl Med*. 2008;49:517-523.

38. Mankoff DA, Dunnwald LK, Gralow JR et al. Blood flow and metabolism in locally advanced breast cancer: relationship to response to therapy. *J Nucl Med*. 2002;43:500–509.

39. Verfaillie SC, Adriaanse SM, Binnewijzend MA et al. Cerebral perfusion and glucose metabolism in Alzheimer's disease and frontotemporal dementia: two sides of the same coin? *Eur Radiol*. 2015;25:3050-3059.

40. Musiek ES, Chen Y, Korczykowski M et al. Direct comparison of fluorodeoxyglucose positron emission tomography and arterial spin labeling magnetic resonance imaging in Alzheimer's disease. *Alzheimers Dement*. 2012;8:51-59.

41. Olesen BW. Technical Review No. 2. Thermal Comfort. Bruel & Kjaer 1982, Accessed on http://www.bksv.com/doc/TechnicalReview1982-2.pdf

42. Abreu-Vieira G, Hagberg CE, Spalding KL, Cannon B, Nedergaard J. Adrenergically stimulated blood flow in brown adipose tissue is not dependent on thermogenesis. *Am J Physiol Endocrinol Metab*. 2015;308:E822-829.

43. Foster DO, Frydman ML. Nonshivering thermogenesis in the rat. II. Measurements of blood flow with microspheres point to brown adipose tissue as the dominant site of the calorigenesis induced by noradrenaline. *Can J Physiol Pharmacol*. 1978;56:110-122.

44. Ukropec J, Anunciado RP, Ravussin Y, Hulver MW, Kozak LP. UCP1-independent thermogenesis in white adipose tissue of cold-acclimated Ucp1-/- mice. *J Biol Chem*. 2006;281:31894-31908.

45. Wijers SL, Schrauwen P, van Baak MA, Saris WH, van Marken Lichtenbelt WD. Beta-adrenergic receptor blockade does not inhibit cold-induced thermogenesis in humans: possible involvement of brown adipose tissue. *J Clin Endocrinol Metab*. 2011;96:E598-605.

46. Bal NC, Maurya SK, Sopariwala DH et al. Sarcolipin is a newly identified regulator of muscle-based thermogenesis in mammals. *Nat Med*. 2012;18:1575-1579.

47. Kashiwazaki H, Dejima Y, Suzuki T. Influence of upper and lower thermoneutral room temperatures (20 degrees C and 25 degrees C) on fasting and post-prandial resting metabolism under different outdoor temperatures. *Eur J Clin Nutr*. 1990;44:405-413.

48. Plasqui, G, Kester ADM, Westerterp KM. Seasonal variation in sleeping metabolic rate, thyroid activity, and leptin. *Am J Physiol*. 2003; 285:E338–E343.

49. Leonard WR, Levy SB, Tarskaia TA, Klimova TM, Fedorova VI, Baltakhinova ME, Krivoshapkin VG, Snodgrass JJ. Seasonal variation in basal metabolic rates among the Yakut (Sakha) of northeastern Siberia. *Am J Hum Biol*. 2014;26:437-445.

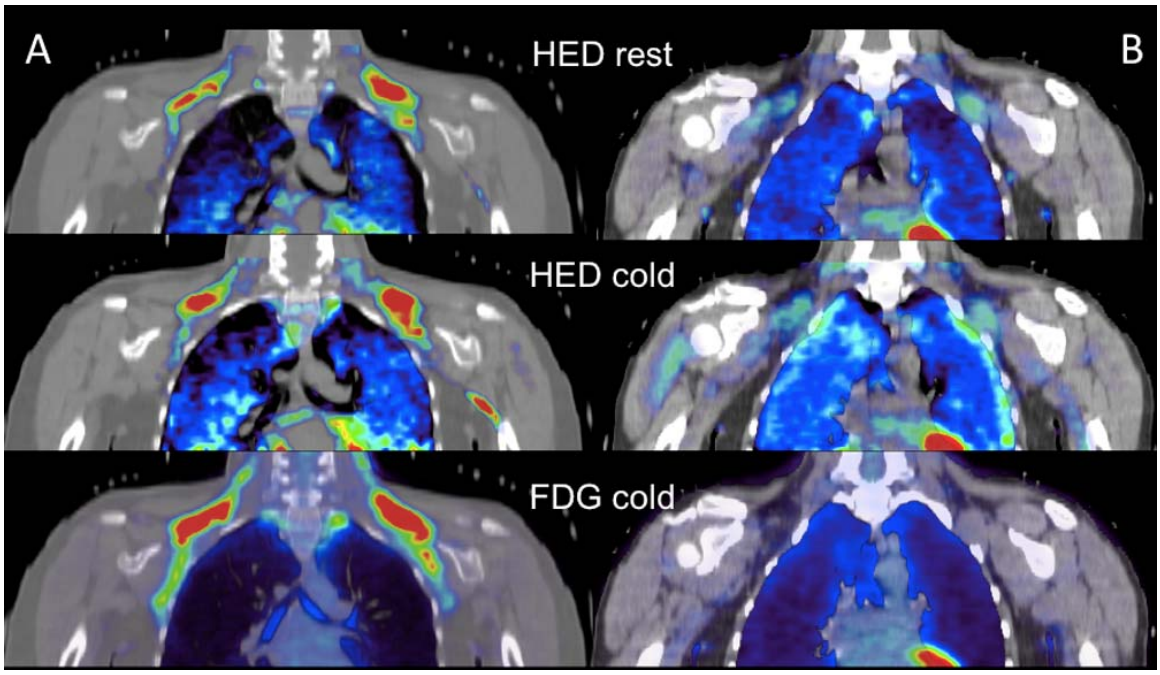

Figure 1. HED PET tracer uptake in supraclavicular BAT (arrows) during thermoneutral condition (HED rest, upper row), during cold exposure (HED cold, middle row) as well as FDG tracer uptake during cold exposure (FDG cold, bottom row) in a subject with cold-activated BAT (A) and a subject without cold-activated BAT (B).

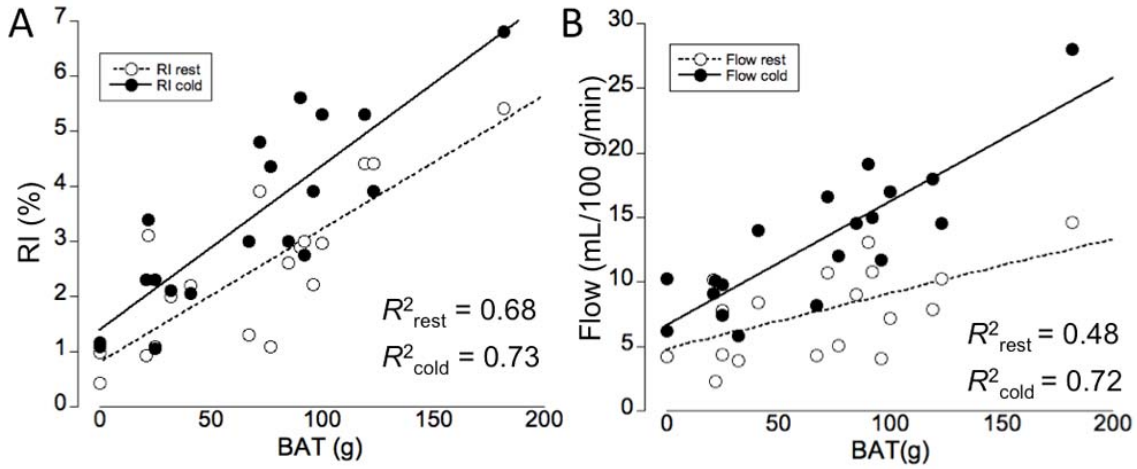

Figure 2. Linear relationship between supraclavicular BAT mass and HED RI at both rest and cold (A) as well as between BAT mass and blood flow in BAT (B). The graphs indicate linear relationships between the HED RIs and BAT mass at both conditions as well as between BAT mass and blood flow.

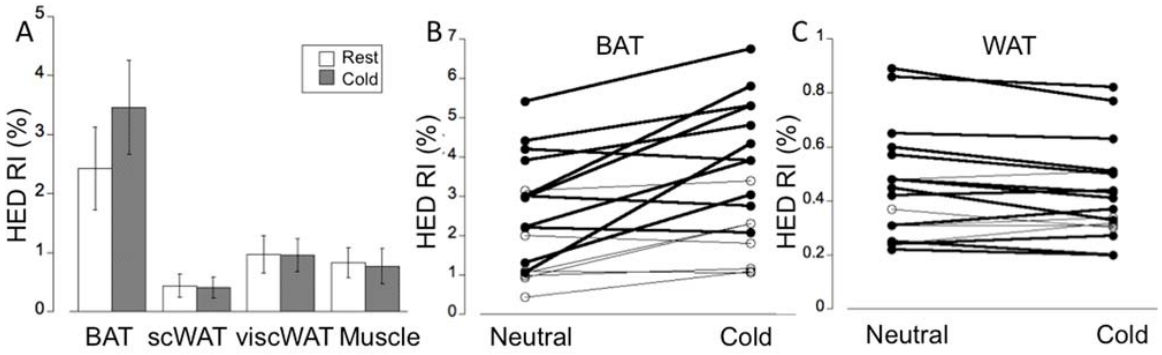

Figure 3. (A) HED PET tracer uptake quantified using the retention index (RI) defined as the tracer concentration in tissue at 30min p.i. divided by the integral of the blood input function from 0 – 30min. The graph demonstrates an overall significant increase in RI at the location of supraclavicular BAT (BAT), but not at subcutaneous WAT (WAT) and visceral WAT (viscWAT). (B) Variable increase in RI following cold exposure determined at the location of supraclavicular WAT. (C) In contrast, RI in subcutaneous WAT (WAT) shows a consistent decrease following cold exposure.

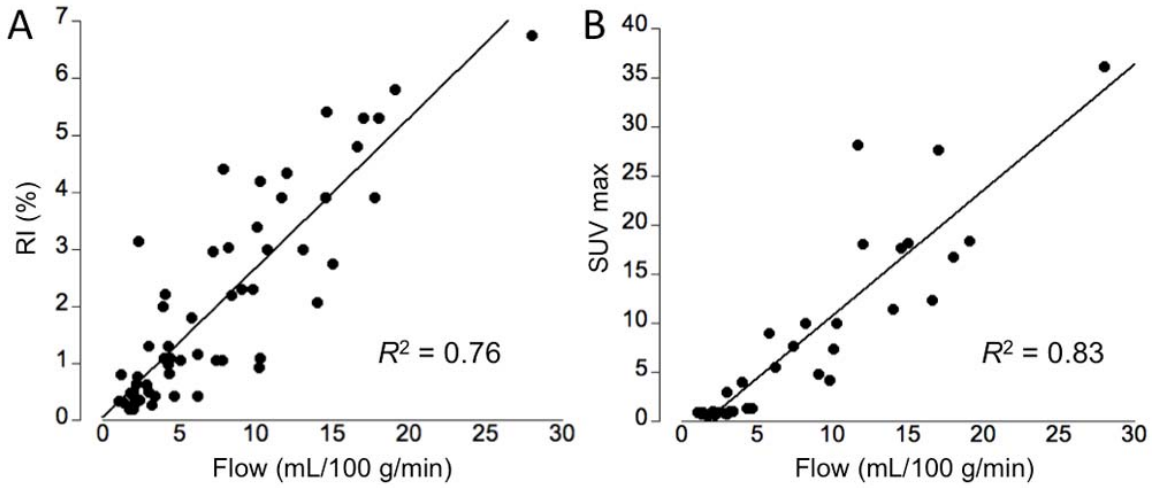

Figure 4. (A) Linear relationship between blood flow (ml/100g/min) and sympathetic innervation as measured using the RI (%) at the location of supraclavicular BAT and subcutaneous WAT during both rest and cold exposure. (B) Linear relationship between blood flow and SUVmax at the location of supraclavicular BAT and subcutaneous WAT during cold exposure.

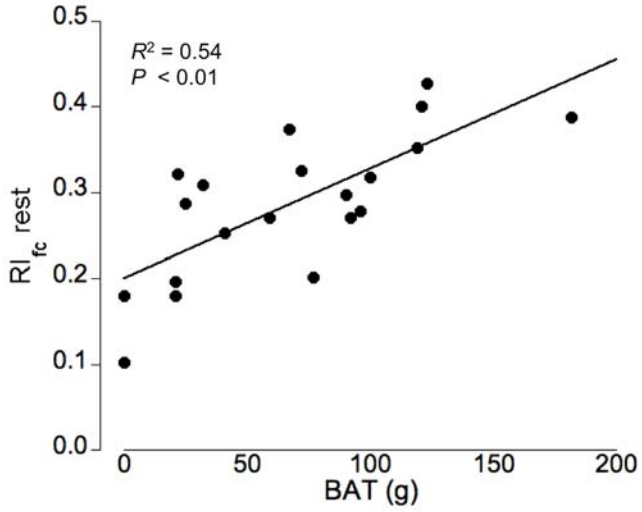

Figure 5. Significant relationship between flow-corrected HED retention index (RI_{fc}) at thermoneutral condition (rest) and cold-activated BAT mass ($p < 0.01$).

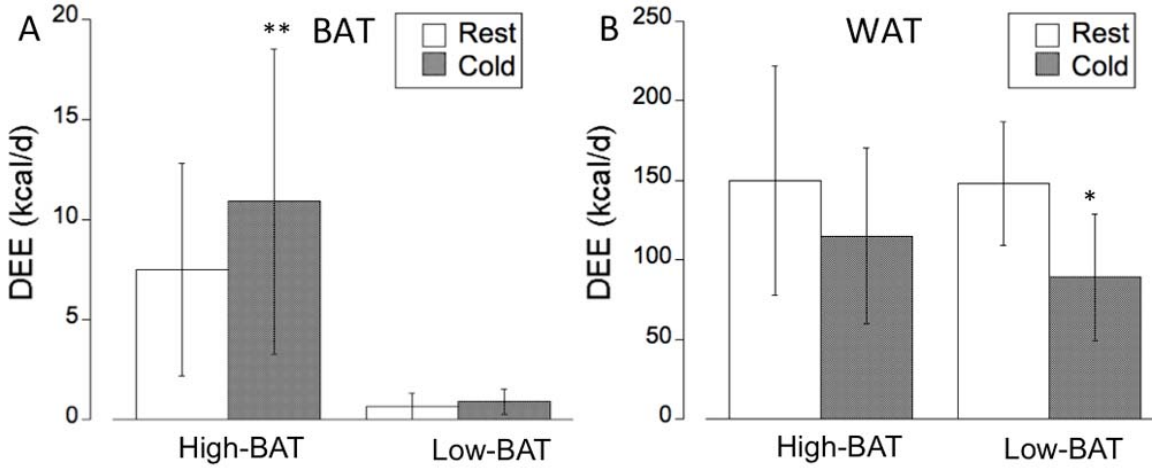

Figure 6. (A) Contribution of supraclavicular BAT (BAT) determined in our subject group to daily energy expenditure (DEE) at thermoneutral (rest) and cold condition. The graph indicates a small contribution of BAT to whole body DEE in the range of <20kcal/day. (B) In contrast, the contribution of subcutaneous WAT (WAT) to whole body DEE is much higher due to the large WAT mass, although cold exposure results in a substantial decrease in WAT DEE (** $p < 0.01$, * $p < 0.05$).

Table 1. Descriptive Statistics of Subjects in High-BAT and Low-BAT Groups (mean ± SD; p-value between groups).

Parameter	All Subjects	High-BAT	Low-BAT	p-value
Subjects	20 (10F/10M)	13 (8F/5M)	7 (2F/5M)	
Height (cm)	172 ± 12	170 ± 13	175 ± 12	NS
Weight (kg)	69 ± 16	65 ± 16	76 ± 17	NS
BMI (kg/m^2)	23.0 ± 2.6	22.0 ± 2.1	24.8 ± 2.4	0.03
Body Fat (%)	25.4 ± 5.8	25.3 ± 6.3	25.5 ± 5.2	NS
BAT mass (g)	68 ± 49	96 ± 37	16 ± 4	<0.01
WAT mass (kg)	17.4 ± 4.9	16.3 ± 5.5	19.5 ± 3.6	NS
Visc.Fat Area (cm^2)	36.5 ± 19.4	32.3 ± 19.6	44.1 ± 18.1	NS
BAT SUVmax	16.2 ± 8.8	19.5 ± 8.0	7.2 ± 1.7	<0.01
BAT Metab.Act.(g)	468 ± 450	609 ± 451	81 ± 22	<0.01
BAT DEE rest (kcal/d)	1469 ± 401	1349 ± 403	1712 ± 337	NS
Δ WB DEE (kcal/d)	223 ± 396	340 ± 380	9 ± 361	NS
Δ WB DEE (%)	10.5 ± 21.3	17.1 ± 16.5	0.8 ± 23.4	NS

Table 2. HED RI in supraclavicular BAT (BAT), subcutaneous WAT (WAT) and visceral WAT (viscWAT) at thermoneutral and cold condition observed in the High-BAT and Low-BAT groups (mean ± SD; p-value between groups).

Parameter	All Subjects	High-BAT	Low-BAT	p-value
RI rest (BAT)	2.42 ± 0.85	3.05 ± 1.0	1.42 ± 0.6	<0.01
Ri cold (BAT)	3.43 ± 0.93*	4.27 ± 1.1*	1.91 ± 0.6	<0.01
RI rest (WAT)	0.44 ± 0.22	0.46 ± 0.19	0.42 ± 0.23	NS
RI cold (WAT)	0.41 ± 0.18	0.44 ± 0.18	0.38 ± 0.19	NS
RI rest (viscWAT)	0.97 ± 0.32	1.03 ± 0.33	0.87 ± 0.40	<0.01
RI cold (viscWAT)	0.96 ± 0.28	1.00 ± 0.29	0.86 ± 0.34	<0.01

* $p < 0.05$ between rest and cold

Supplemental Data

Supplemental Figure 1

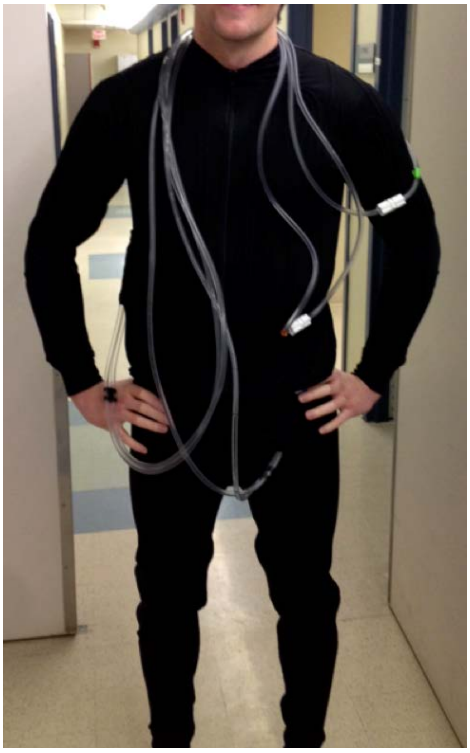

Supplemental Figure 1. Garment used for cold exposure. Subject dressed in the tube suit covering the arms to the wrists, the legs to the ankles and the torso. Plastic tubes were connected to a pump with two water reservoirs, both of which were temperature controlled. The water temperature in the reservoirs was kept constant at 31-34 ^{o}C and 15–17 ^{o}C, respectively.

Supplemental Figure 2

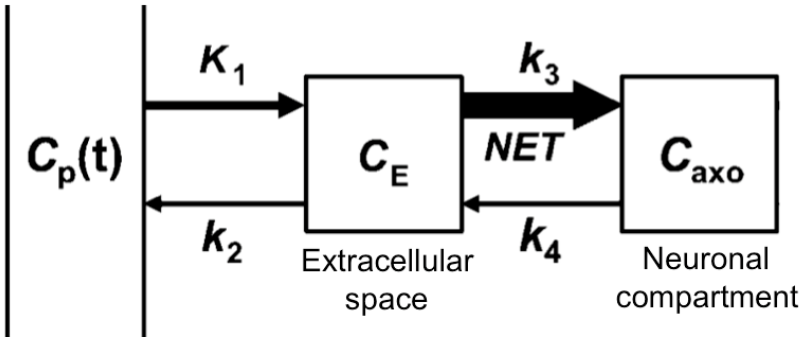

Supplemental Figure 2. Kinetic model for HED. Arrow thicknesses indicate relative magnitudes of the rate constants. Cp represents HED tracer concentration in plasma, CE represents tracer concentration in extracellular space and Caxo represents tracer concentration in the neuronal axoplasm.

Supplemental Figure 3

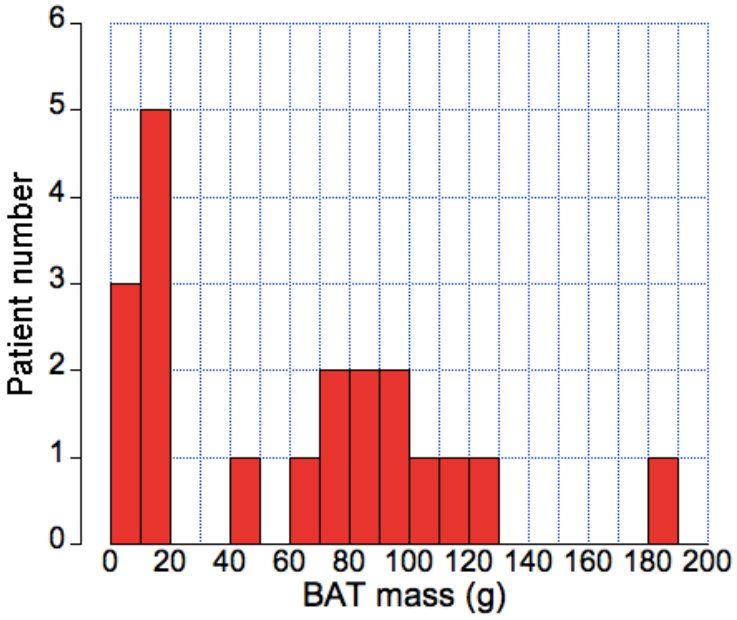

Supplemental Figure 3. Histogram showing the distribution of cold-activated BAT mass in all subjects studied. The graph indicates that a bimodal distribution with two distinct peaks at 10-20g and 80-90g. Based on the data, we have stratified subjects into 2 groups according to their cold-activated BAT mass. A High-BAT group with BAT mass greater than 20g and a Low-BAT group with BAT mass less than 20g.

Supplemental Experimental Procedures.

Study population

Stature was measured to the nearest cm and weight was measured to the nearest 0.5 kg, following standard procedures of Lohman et al. (*1*). The body mass index (BMI) was calculated as weight/height^2 (kg/m^2). Percent body fatness (%) was calculated based on the Durnin and Womersley (*2*) equations from the sum of skinfold measurements at the biceps, triceps, subscapular and suprailiac sites using Lange calipers. The lean body mass (LBM; kg) was subsequently calculated as body weight less fat mass and WAT mass was calculated as body weight multiplied with the body fat percentage.

Cold exposure approach

Mild cold exposure was applied using a specialized whole-body garment, which incorporates a network of small-diameter plastic tubing (Allen Vangard, Inc., Ottawa, CA) (**Supplemental Fig. 1**). The garment incorporates a network of small-diameter plastic tubing through which temperature-controlled neutral (31-34°C) or cold water (15-17°C) was circulated from two separate water reservoirs. Skin temperature was monitored using a GaAs crystal sensor located at the tip of an optical fiber cable (OpSense, Inc., Quebec City, CA), which allows accurate measurement to within 0.1^{o}C. This approach relies on the temperature dependence of the energy band gap of a GaAs semiconductor crystal; the GaAs sensor is opaque for wavelengths below the bandgap and transparent for wavelengths above the energy band gap. The sensor was taped to the skin at the location of the left rib cage. This location was selected on the basis of proximity to important anatomical features (close to the pulmonary blood vessels which are possibly the most representative sites for core body temperature) and the ability to consistently place the sensors based on the anatomical landmark. Previous studies (*3,4*) have shown a strong correlation (R^2 = 0.70) between this location and core body temperature.

Definition of BAT mass

ROIs representing supraclavicular BAT as well as subcutaneous and visceral WAT were defined in CT images based on the density of adipose tissue (−250 to −50 Hounsfield

units, HU). BAT was considered as activated if there were areas of tissue that were more than 5 mm in diameter and had a minimal standard uptake value (SUV, defined as tracer concentration in MBq/cc normalized to injected activity (MBq) per weight (g)) of FDG of at least 2.0. This cutoff represented more than 2 SD above the maximal SUV seen in typical depots of white adipose tissue. In case that no voxels survived the masking operation (no BAT activation), a volume of ~10 cm^3 (1.5 x 1.5 x 4.0 cm^3 ROI) was selected at a typical location of supraclavicular BAT. The final BAT ROI was chosen at the location of the largest contiguous group of voxels that survived the masking operation.

References

1. Lohman TG, Roche AF, Martorel R. Anthropometric standardization reference manual. Champaign, IL; Human Kinetics Books, 1988

2. Durnin JVA, Womersley J. Body fat assessed from the total body density and its estimation from skinfold thickness: measurements on 481 men and women aged from 16 to 72 years. Br J Nutr 1974; 32:77-97

3. Xu X, Karis AJ, Buller MJ, Santee WR. Relationship between core temperature, skin temperature, and heat flux during exercise in heat. Eur J Appl Physiol 2013; 113: 2381–2389.

4. Yamakage M, Namiki A. Deep temperature monitoring using a zero-heat-flow method. J Anesth. 2003; 7: 108-15.